

See discussions, stats, and author profiles for this publication at: <https://www.researchgate.net/publication/256428502>

# Minimal Model for Self-Catalysis in the Formation of Amyloid-Like Elongated Fibrils

ARTICLE *in* JOURNAL OF PHYSICAL CHEMISTRY LETTERS · SEPTEMBER 2013

Impact Factor: 7.46 · DOI: 10.1021/jz401600g

---

CITATIONS

3

---

READS

28

3 AUTHORS, INCLUDING:



Erika Eiser

University of Cambridge

56 PUBLICATIONS 1,014 CITATIONS

SEE PROFILE



Vito Foderà

University of Copenhagen

25 PUBLICATIONS 321 CITATIONS


SEE PROFILE

# Minimal Model for Self-Catalysis in the Formation of Amyloid-Like Elongated Fibrils

Lorenzo Di Michele,<sup>†</sup> Erika Eiser,<sup>†</sup> and Vito Fodera<sup>\*,†,‡</sup>

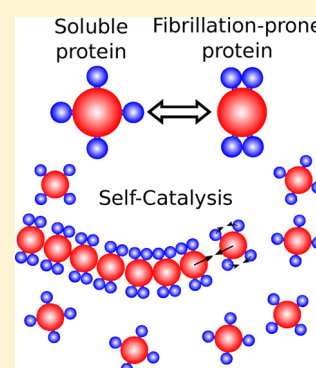
<sup>†</sup>Sector of Biological and Soft Systems (BSS), Department of Physics, Cavendish Laboratory, University of Cambridge, Cambridge CB3 0HE, United Kingdom

<sup>‡</sup>Department of Drug Design and Pharmacology, Faculty of Health and Medical Sciences, University of Copenhagen, 2100 Copenhagen, Denmark

 Supporting Information

**ABSTRACT:** Understanding the mechanism behind protein aggregation is a challenging task that requires a combined use of both experimental and computational approaches. In this work, we present a 2D model for the formation of amyloid-like fibrils. The model allows one to explicitly consider the structural change of the native state of a protein into the aggregation-prone state together with the overall charge of the molecules. By means of Metropolis Monte Carlo and dynamic Monte Carlo, we simulate both the equilibrium and kinetic behavior of an ensemble of model proteins. Our results show the effect of the charge and protein concentration on both the conformational equilibrium and the kinetics of the aggregation process. Specifically, the model is capable of capturing the self-catalytic conversion of native proteins into aggregation-prone ones in the presence of preexisting aggregates, naturally reproducing some peculiar scaling laws observed for a class of amyloidogenic systems.

**SECTION:** Biophysical Chemistry and Biomolecules



**E**lucidation of the multistep process leading a native protein to convert into an amyloid aggregate is a crucial point in current biophysical research. The large interest in this topic is mainly due to the still unclear connection between the amyloid deposits found in human tissues and the onset of pathologies as Alzheimer's and Parkinson's disease.<sup>1,2</sup> Protein deposits are mainly formed by elongated amyloid fibrils that are characterized by a common cross- $\beta$  structure, possibly presenting different isoforms.<sup>3</sup>

Oligomeric precursors of the fully developed fibrils are thought to be responsible for the toxicity of the amyloid aggregates. Special attention has therefore been devoted to investigations of the thermodynamics and kinetics of the early stages of the fibrillar growth.<sup>4–16</sup> The difficulties encountered in the experimental characterization of the oligomer nucleation and growth<sup>17,18</sup> promoted the use of computational approaches. However, fully atomistic or poorly coarse-grained models are not suitable for this purpose due to the need of simulating systems with a relatively large number of proteins over time windows well above 1  $\mu$ s. Several coarse-grained models, more or less reminiscent of the physical structure of the proteins, have been proposed to overcome this limitation.<sup>4–11,19</sup> One of the basic features of successful models is the possibility for single proteins to fluctuate between two internal states, that is, the monomeric and the aggregation-prone state. The transition between the two states mimics the conformational change between the soluble and the amyloidogenic internal structures of fibril-forming proteins.

The two general scenarios mainly accepted to explain the delayed (sigmoidal) growth curves observed at early stages of protein fibrillation are (i) a nucleated polymerization process, in which the time-limiting step consists of the association of a critical number of fibrillation-prone monomers present in solution and (ii) a templated growth process in which the time-limiting step is governed by the conversion of soluble monomers into fibril-prone proteins,<sup>16</sup> for example, conformational changes.

The level of detail and the assumptions in a model for protein fibrillation are mainly dictated by the specific aspects under investigation. In the model by Vacha and co-workers,<sup>9,11</sup> the conformational change is taken into account by a two-state internal degree of freedom that controls the strength and the size of an attractive patch mediating the aggregation of hard spherocylinders. This choice has previously been applied to the case of spheres with isotropic attraction<sup>7</sup> and successfully accounts for a variety of aggregate structures. However, it does not capture the explicit changes in the shape of the building blocks, which are necessary if one aims to properly describe the early events and the subsequent templated growth. In the model proposed by Cafish and Pellarin,<sup>4–6</sup> the conformational change is associated with the rotation of a dihedral angle in an otherwise rigid assembly of 10 beads. The rotation determines

**Received:** July 27, 2013

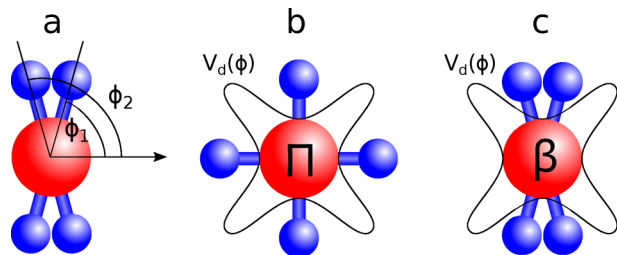
**Accepted:** September 3, 2013

different states with different internal energies. However, such an ad hoc geometrical switch is not explicitly connected with physicochemical properties of the solution that are generally controlled during in vitro experiments.

In this Letter, we present a minimal off-lattice model specifically designed for amyloid-like fibril formation that exhibits an explicit conformational transition between a soluble ( $\Pi$ ) and an amyloidogenic ( $\beta$ ) configuration. Hydrophobicity of the protein core and the charging state of side chains are crucial in determining the fibril-like structures,<sup>20,21</sup> and we explicitly take them into account, with the  $\Pi$ – $\beta$  transition being influenced by the charging state of the hydrophilic parts of the protein. Fibrillation propensity, self-catalysis, and kinetics are then investigated as a function of physicochemical parameters generally controlled during experiments. For the sake of simplicity, we introduce a two-dimensional model, though a 3D generalization is possible and will be the object of future investigations. We study the equilibrium features of the model by means of Metropolis Monte Carlo (MC) simulations and the fibrillation dynamics by means of dynamic Monte Carlo.

As shown in Scheme 1, our model protein consists of a hydrophobic core (red bead) with radius  $R_H$  that interacts with

**Scheme 1. Scheme of the Model Protein<sup>a</sup>**



<sup>a</sup>For clarity, the diameter of the beads representing charged and hydrophobic parts is smaller than their actual size. The blue rods connecting the charged beads have only a graphical purpose. (a) Definition of the two internal coordinates. (b) Protein in the  $\Pi$  configuration. (c) Protein in the  $\beta$  configuration. The curve in panels b and c sketches the internal potential felt by single dumbbells.

other hydrophobic cores via a truncated and shifted Lennard-Jones (LJ) potential

$$V_h(r) = \begin{cases} 4\epsilon_h \left[ \left( \frac{R_h}{r} \right)^{12} - \left( \frac{R_h}{r} \right)^6 \right] - V_{hc} & \text{if } r < R_C \\ 0 & \text{if } r \geq R_C \end{cases} \quad (1)$$

where  $V_{hc} = 4\epsilon_h[(R_h/R_C)^{12} - (R_h/R_C)^6]$ . Four charged spheres (blue beads) surround the core at distance  $R_h$  from the center. Charged beads, mimicking hydrophilic groups, interact via a screened Coulomb interaction modeled as a truncated-shifted Yukawa potential

$$V_g(r) = \begin{cases} Z_i Z_j \frac{e^{-r/\lambda}}{r} - V_{gc} & \text{if } r < R_C \\ 0 & \text{if } r \geq R_C \end{cases} \quad (2)$$

where  $V_{gc} = Z_i Z_j \exp(-R_C/\lambda)/R_C$ ,  $Z_i$  and  $Z_j$  are the charges, and  $\lambda$  is the Debye screening length. Here, we make the simplifying assumption that the charges on the four hydrophilic beads are equal in sign and magnitude; therefore,  $Z_i = Z_j = Z$ .

A steric repulsion, described by a Weeks–Chandler–Andersen potential, is present between groups belonging to one protein and group/cores belonging to other proteins

$$V_{gg/gc}(r) = \begin{cases} 4\epsilon_{gg/gc} \left[ \left( \frac{R_{gg/gc}}{r} \right)^{12} - \left( \frac{R_{gg/gc}}{r} \right)^6 \right] + \frac{1}{4} & \text{if } r < 2^{1/6} R_{gg/gc} \\ 0 & \text{if } r \geq 2^{1/6} R_{gg/gc} \end{cases} \quad (3)$$

where the labels gg and gc refer to group–group and group–core interactions, respectively.

The position of the two pairs of charged beads is constrained to form two rigid dumbbells, the axes of which form angles  $\phi_1$  and  $\phi_2$  with respect to the internal frame of reference of proteins, as sketched in Scheme 1 a. The dumbbells are subject to an internal potential

$$V_d(\phi_1, \phi_2) = \epsilon_d \left[ \sin^2\left(\frac{\phi_1}{2}\right) + \sin^2\left(\frac{\phi_2}{2}\right) \right] \quad (4)$$

that tends to stabilize configurations for which  $\phi_1 \approx n(\pi/2)$  and  $\phi_2 \approx m(\pi/2)$ ;  $n$  and  $m$  are two integers.

MC equilibrium simulations are performed within a square box of size  $L$  with periodic boundary conditions, a constant number of proteins  $N$ , and temperature  $T$ . Further details on the model, the definition of the reduced units, and the numeric value of the parameters used are provided in the Methods section.

In the absence of Coulomb repulsion between the charged beads, eq 4 describes the internal energy of a single protein, which is plotted in Figure 1a (panel with  $Z = 0$ ). Among the four (periodically repeated) equivalent minima, we can distinguish two  $\Pi$  regions, where  $\phi_1 \approx \phi_2 + n\pi/2$ , and two  $\beta$  regions, where  $\phi_1 \approx \phi_2 + n\pi$ .

In configuration  $\Pi$ , the axes of the dumbbells are perpendicular to each other (Scheme 1b), preventing the hydrophobic cores of approaching proteins from getting in close contact and, therefore, hindering aggregation. In configuration  $\beta$ , the dumbbells align almost parallel to each other (Scheme 1c), leaving two accessible hydrophobic patches on opposite sides of the protein and enabling aggregation, as demonstrated in the simulation snapshots in Figure 1b.

Taking into account the Coulomb repulsion (i.e.,  $Z > 0$ ), the internal potential energy of the dumbbells is

$$V_{int}(\phi_1, \phi_2) = V_d(\phi_1, \phi_2) + 2Z^2 \left[ \frac{e^{-d_1/\lambda}}{d_1} + \frac{e^{-d_2/\lambda}}{d_2} \right] \quad (5)$$

with  $d_1 = |2R_g \cos[(\phi_1 - \phi_2)/2]|$  and  $d_2 = |2R_g \sin[(\phi_1 - \phi_2)/2]|$ . As shown in Figure 1a, configurations  $\beta$  become metastable for  $Z > 0$ . For highly charged proteins, the amyloidogenic configurations eventually become unstable for isolated monomers within the ensemble, and the only energy minima are those of the  $\Pi$  states.

To quantitatively describe the above-mentioned tendency, we perform MC simulations at different values of  $Z$ . In Figure 1c, we show, for a single protein, the probability  $P_\beta$  of occupying  $\beta$  configurations. We assume that the protein is in the  $\beta$  configuration when  $\phi_1 \in [0, \pi/4) \cup [3\pi/4, 5\pi/4) \cup [7\pi/4, 2\pi)$  and  $\phi_2 \in [\pi/4, 3\pi/4) \cup [5\pi/4, 7\pi/4)$ , or vice versa. Otherwise, the protein is assumed to be in the  $\Pi$  configuration. Regions belonging to  $\Pi$  and  $\beta$  configurations according to this definition are shown in Figure 1a (panel with  $Z = 0$ ).

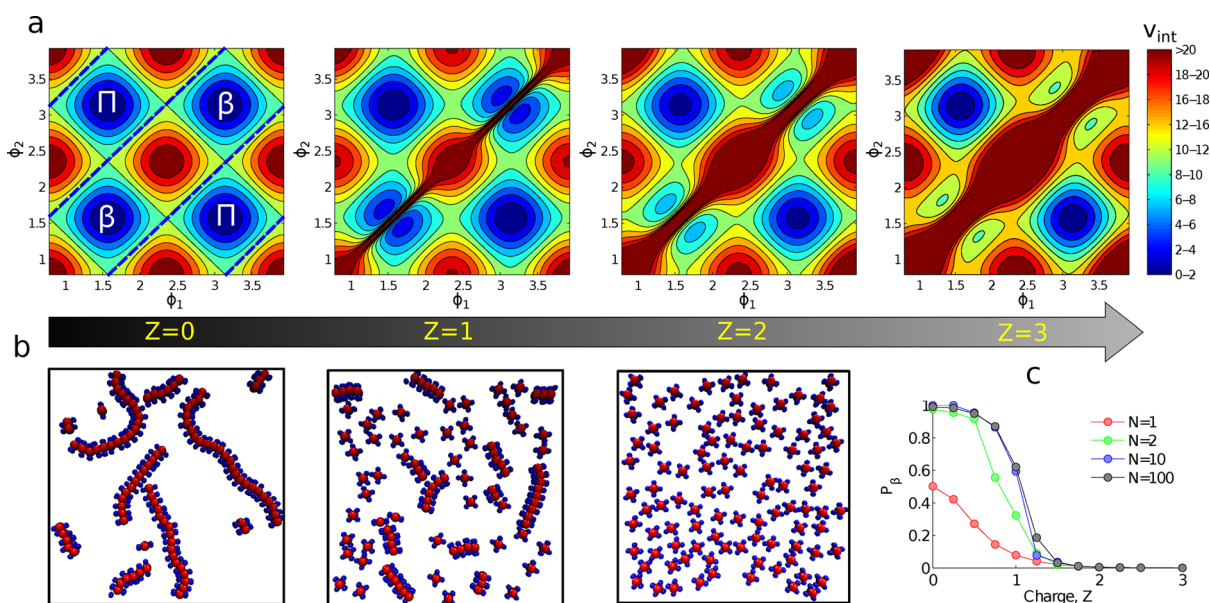


**Figure 1.** (a) Total internal energy of an isolated protein as a function of the dumbbells coordinates  $\phi_1$  and  $\phi_2$  as expressed by eq 5 for various  $Z$ . Blue dashed lines in the  $Z = 0$  panel separate  $\beta$  from  $\Pi$  regions. (b) Snapshot from an equilibrium MC simulation of systems with  $N = 100$ ,  $\rho = 0.005$ , and various  $Z$ . (c) Probability of  $\beta$  configurations sampled from equilibrium MC simulations for various  $N$  as a function of  $Z$ .

As expected for  $Z = 0$ , we find  $P_\beta = 1/2$ , that is,  $\beta$  and  $\Pi$  configurations are equally likely. When the charge increases,  $P_\beta$  rapidly decays to 0, highlighting the instability of the  $\beta$  configuration.

However, results obtained for a single protein are not comparable to the experiments, where the protein–protein interaction can affect the conformational stability. To characterize the role played by multiple-body effects, we sample  $P_\beta$  in ensembles containing an increasing number of proteins. The results are shown in Figure 1c. When  $P_\beta$  is sampled for a system containing two proteins, we observe  $P_\beta \approx 1$  for small values of  $Z$ . When the two proteins form a dimer, the potential energy gain due to the core–core attraction compensates for the higher internal energy of the  $\beta$  configurations, stabilizing the proteins in the amyloidogenic state. The dependence of  $P_\beta(Z)$  on the number of proteins  $N$  in the system saturates already at  $N = 10$ .

The mutual stabilization of the proteins in the  $\beta$  state results in a sharp transition from the low- $Z$  regime in which  $P_\beta(Z) \approx 1$  to the high- $Z$  regime in which  $P_\beta(Z) \approx 0$ . In the latter regime, the formation of fibrils is hindered (Figure 1c).

The fact that, in the presence of an ensemble of proteins, a high probability of occurrence of the  $\beta$  state is obtained even at  $Z \neq 0$  is in line with the observations made for a number of proteins that show a pronounced propensity for undergoing conformational changes at a pH far from their pI (isoelectric point), where a single protein carries a net charge.<sup>22–24</sup>

To verify whether the combination of conformational changes and the mutual stabilization of fibrillation-prone proteins is capable of accurately mimicking amyloid aggregation, we consider systems containing  $N = 625$  proteins. We sample the equilibrium normalized mass concentration of the aggregates  $P(n) = nN_n/N$ , where  $N_n$  the number of fibrils of length  $n$ . In particular, we keep track of the monomers', dimers', and trimers' mass concentrations  $P(1)$ ,  $P(2)$ , and  $P(3)$ . We classify species larger than a trimer as a fibril and define the fibrils' mass concentration as  $P_{\text{fib}} = \sum_{n=4}^N P(n)$ .

In the phase diagram shown in Figure 2a, we indicate the predominant (in term of mass concentration) species as a

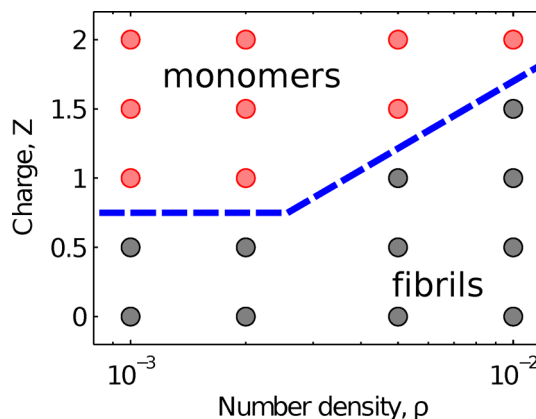


**Figure 2.** Phase diagram showing the predominant species in terms of the normalized mass distribution as a function of  $\rho$  and  $Z$ . Red symbols indicate a predominance of monomers,  $P(1) > P(2), P(3), P_{\text{fib}}$ . Gray symbols indicate a predominance of fibrils,  $P_{\text{fib}} > P(1), P(2), P(3)$ .

function of  $Z$  and the number density  $\rho = N/L^2$ . With red symbols, we indicate a predominance of monomers,  $P(1) > P(2), P(3), P_{\text{fib}}$ ; with gray symbols, we indicate a predominance of fibrillar aggregates,  $P_{\text{fib}} > P(1), P(2), P(3)$ . We find a sharp boundary between the fibrillation-prone regime, for high  $\rho$  and low  $Z$ , and the soluble monomer regime, for high  $Z$  and low  $\rho$ . The oligomeric intermediates (dimers and trimers) are never found to be the stable species at the equilibrium. It is worth noting that at increasing  $\rho$ , the formation of fibrils is accessible also at higher values of  $Z$ . This is experimentally observed for concentrated protein systems (both model and medically relevant) in which formation of amyloid fibrils, often accompanied with large-scale rearrangement, is observed at a pH far from the pI of the protein.<sup>25–27</sup> The equilibrium normalized mass distribution showing the relative abundance of



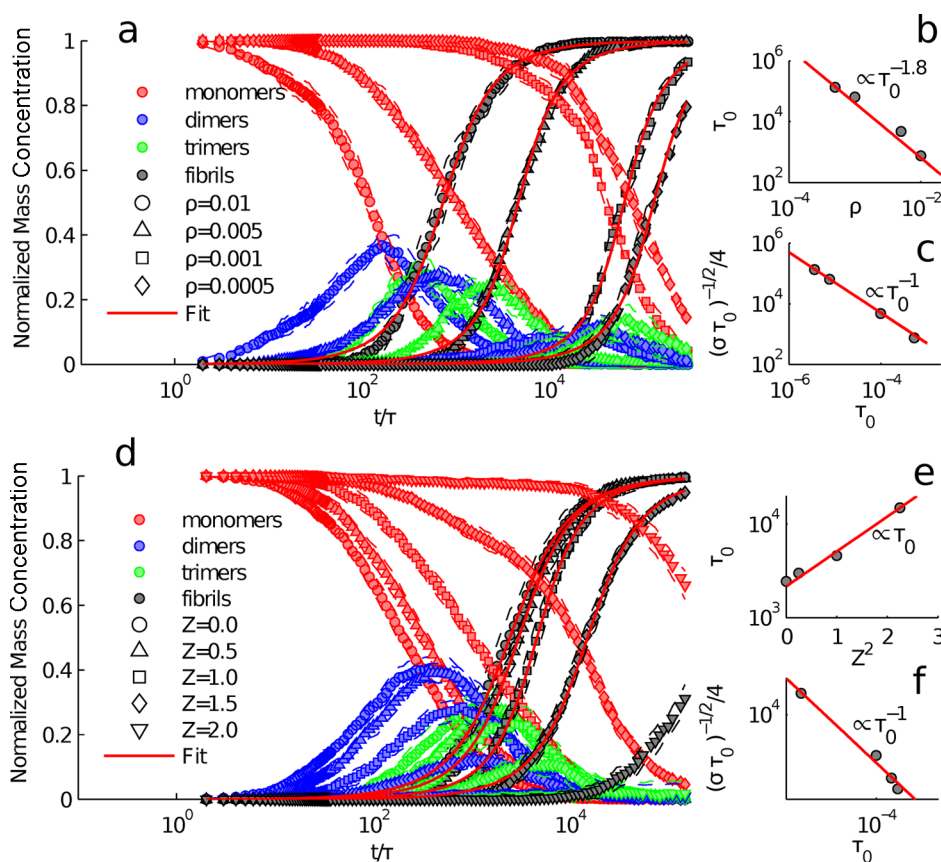


**Figure 3.** (a) Evolution of the normalized mass distributions for  $Z = 1.0$ ,  $\epsilon_h = 16$ , and various values of  $\rho$ . Red solid lines represent fits according to eq 6. (b) Fitted values of  $\tau_0$  as a function of  $\rho$  for the curves shown in panel a. The red solid line is a power law fit with exponent  $-1.8$ . (c) Fibrillar growth rate  $(\sigma\tau_0)^{-1/2}/4$  as a function of  $\tau_0$  for the curves shown in panel a. The red solid line is a power law fit with exponent  $-1$ . (d) Evolution of the normalized mass distributions for  $\rho = 0.005$ ,  $\epsilon_h = 16$ , and various values of  $Z$ . Red solid lines represent fits according to eq 6. (e) Fitted values of  $\tau_0$  as a function of  $Z^2$  for the curves shown in panel d. The red solid line is a power law fit with exponent  $1$ . (f) Fibrillar growth rate  $(\sigma\tau_0)^{-1/2}/4$  as a function of  $\tau_0$  for the curves shown in panel d. The red solid line is a power law fit with exponent  $-1$ . Each curve in panels a and d is averaged over 16 replicas of ensembles with  $N = 324$ ; dashed lines indicate the standard deviation.

$n$ -mers, including those with  $n > 3$ , is displayed in Figure S1 (Supporting Information) for various values of  $\rho$  and  $Z$ .

With the aim of investigating the effect of charge and protein concentration on the fibrillation kinetics, we perform dynamic MC simulations (see the Methods section). Specifically, we sample  $P(1)$ ,  $P(2)$ ,  $P(3)$ , and  $P_{\text{fib}}$  as a function of time. The mass distribution curves are averaged over 16 independent replicas with  $N = 324$  proteins each.

In Figure 3a, we show the effect of the protein concentration  $\rho$  on the fibrillation kinetics for systems with  $Z = 1.0$  and  $\epsilon_h = 16$ . We notice a substantial increase of the delay in the fibrillation process when  $\rho$  is decreased. To quantify the delay, we fit the  $P_{\text{fib}}$  with the empirical function

$$P(t) = \frac{1}{2} + \frac{t - \tau_0}{2\sqrt{(t - \tau_0)^2 + 4\sigma t}} \quad (6)$$

where  $\tau_0$  is the fibrillation half time. In Figure 3b, we show the fitted values of  $\tau_0$  as a function of  $\rho$ , which, as expected for fibrillation processes, follow a power law scaling.<sup>28,29</sup> The relatively high scaling exponent (i.e.,  $\approx -1.8$ ) indicates the predominance of self-catalytic effects, as discussed below.

In Figure 3d, we show the normalized mass concentration curves calculated at fixed  $\rho = 0.005$  and  $\epsilon_h = 16$  and variable  $Z$ . We find a delay in the fibrillation process with increasing  $Z$ . Such a result is not surprising. In fact, in the case of medically

relevant proteins such as  $A\beta^{30}$  and  $\alpha$ -synuclein<sup>31,32</sup> in the regime of low protein concentration, the propensity of forming amyloid fibrils drastically decreases at increasing charging state of the native molecule. However, it is worth noting that such a trend can change in the presence of high conformational flexibility of the protein<sup>33</sup> or pathways leading to nonconventional superstructures.<sup>34</sup> The fitted  $\tau_0$  show an approximate linear dependence of the strength of the Coulomb repulsion  $\propto Z^2$  (Figure 3e). This is a consequence of the increase in the potential barrier separating  $\Pi$  and  $\beta$  configurations.

In Figure 3c and f, we show the relation between the fibrillation half time  $\tau_0$  and the time derivative of  $P_{\text{fib}}$  calculated at the inflection point

$$\left(\frac{\partial P}{\partial t}\right)_{t=\tau_0} = \frac{1}{4\sqrt{\tau_0\sigma}} \quad (7)$$

that provides an estimation of the fibrillar growth rate. For all cases, we find an inverse proportionality between the  $\tau_0$  and  $(\sigma\tau_0)^{-1/2}/4$ . This implies that our model accounts for the kinetic correlation between the two main steps of the process; when the nucleation is faster (i.e., shorter lag time), a very rapid growth phase occurs. Such a correlation has been experimentally measured for proteins with significantly different polypeptide sequences, being accepted as a general feature of the amyloid aggregation process.<sup>35</sup>

Interestingly, changing the strength of the hydrophobic interaction (i.e.,  $\epsilon_h$ ) at fixed  $\rho = 0.005$  and  $Z = 1.0$  does not change substantially the evolution of the normalized mass distributions but only affects the equilibrium values (Figure S2 in the Supporting Information).

Regardless of the core–core attraction strength, the charge, or the density, the oligomeric species are only found as unstable intermediates during the fibrillation process; both  $P(2)$  and  $P(3)$  decay to zero at long times. In all of the cases in which the fibrillation is triggered with large delay, that is, for low  $\rho$  and high  $Z$ , we find a substantial reduction in the mass fraction of the oligomeric intermediates, that is, very few dimers or trimers are found to appear at any stage of the fibrillation process. This indicates a transition between two regimes, (i) for low  $Z$  and/or high  $\rho$ , in which many oligomers nucleate at the same time, and (ii) for high  $Z$  and/or low  $\rho$ , in which the nucleation of the aggregates is rare and only one or very few oligomers nucleate and grow into fibrils. In conditions favorable to fibrillation, relatively large aggregates are found to rapidly grow. This is demonstrated in Figure S3 (Supporting Information), where we show evolution of the normalized mass concentration of  $n$ -mers with  $n = 1, \dots, 19$  for an ensemble with  $\rho = 0.01$  and  $Z = 1.0$ .

In Figure 1c, we have demonstrated that the mutual stabilization of proteins in the  $\beta$  state is crucial for the formation of fibrils; even though  $\beta$  configurations are always metastable compared to  $\Pi$  configurations for  $Z > 0$ , they become stable within the aggregates. This *equilibrium* cooperativity can be obtained also with models in which the soluble-to-amyloidogenic transition of the monomers is described by an internal degree of freedom, without an explicit structural change.

In our model, however, the presence of fibrillation-prone monomers also affects the kinetics of fibrillar growth by facilitating the  $\Pi$ – $\beta$  transition of neighboring monomers in the soluble state. To quantify this effect, we measure the  $\Pi$ – $\beta$  transition rate, initially for a single isolated protein. This is done by initializing the protein in a  $\Pi$  state, with  $\phi_1 = 0$  and  $\phi_2 = \pi/2$ , and then sampling the probability distribution  $f(\tau_{\text{flip}})$  of the flip times  $\tau_{\text{flip}}$  spent to overcome the potential barrier separating  $\Pi$  and  $\beta$  configurations.  $f(\tau_{\text{flip}})$  curves show an exponential trend that we fit with the function  $f_0 \exp(-\kappa_1 \tau_{\text{flip}})$ . The single protein flip rate  $\kappa_1$  calculated as a function of  $Z$  is shown in Figure 4a. As expected, it decays to 0 for high  $Z$  due to the increase of the potential barrier between  $\Pi$  and  $\beta$  states. This partially explains the delay in fibrillation for highly charged proteins.

To investigate the kinetics of self-catalysis, we calculate the flip rate  $\kappa_2^{\text{free}}$  for a single protein in the presence of a second one. Both proteins are initialized in the  $\Pi$  configuration with freely moving dumbbells. In Figure 4b, we see that for low  $Z$ ,  $\kappa_2^{\text{free}}$  is slightly larger than  $\kappa_1$ , but the  $\kappa_2^{\text{free}}/\kappa_1$  ratio decays to 1 for large  $Z$ , as shown in Figure 4d. This indicates that interactions between neighboring soluble monomers play a key role in accelerating fibrillation. In Figure 4c, we show  $\kappa_2^{\text{seed}}$ , calculated for a single protein initialized in the  $\Pi$  configuration in the presence of a second one, which is kept in a  $\beta$  configuration with  $\phi_1 = 0.1$  and  $\phi_2 = 2\pi - 0.1$ . The ratio  $\kappa_2^{\text{seed}}/\kappa_1$ , shown in Figure 4d, demonstrates that at low  $Z$ , the presence of a  $\beta$  seed increases the flip rate by almost an order of magnitude compared to that in the case of a single protein. In other words, exposed  $\beta$  proteins at the extrema of a preformed oligomer or fibril induce a fast  $\Pi$ – $\beta$  transition in soluble monomers that then stick to the fibril. This means that once the early

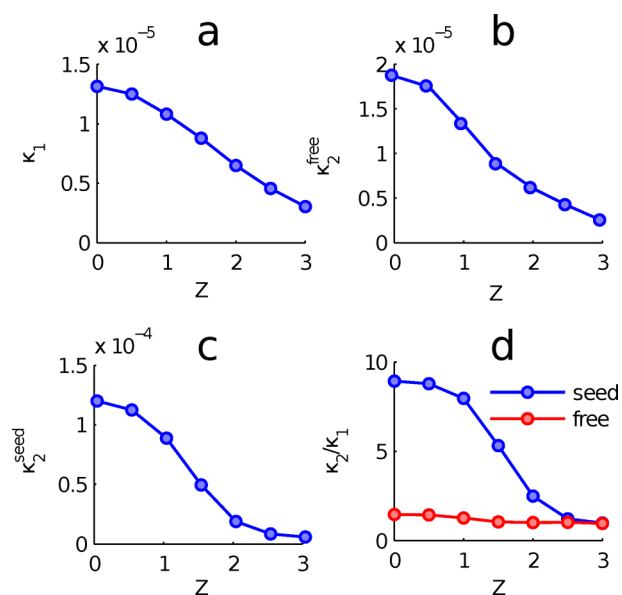


**Figure 4.**  $\beta$ – $\Pi$  flip rate measured as a function of  $Z$  from MC simulations for (a) an isolated protein ( $\kappa_1$ ), (b) a protein in the presence of a second one ( $\kappa_2^{\text{free}}$ ), and (c) a protein in the presence of a second one that is kept in a  $\beta$  configuration ( $\kappa_2^{\text{seed}}$ ). (d) Ratios  $\kappa_2^{\text{free}}/\kappa_1$  and  $\kappa_2^{\text{seed}}/\kappa_1$  as a function of  $Z$ .

aggregates are formed, the  $\Pi$ – $\beta$  transition of a single molecule is triggered by molecules already in the  $\beta$  state (i.e., self-catalysis). This effect is, in our opinion, at the basis of what has been observed experimentally by Jansen and co-workers in the case of insulin fibril formation<sup>36</sup> and later highlighted for a larger class of amyloidogenic systems.<sup>28</sup> For these systems, in the proximity of the fibrillar structure, protein monomers can preferentially align, change conformation, and be part of a (new) growing fibril.<sup>36</sup> Such a mechanism, generally known in the literature as secondary nucleation,<sup>37,38</sup> determines in turn the explosive growth of the aggregate size<sup>26–28,39</sup> as also observed and predicted by our model in Figure 3. The presence of such a self-catalytic effect would also fit with the specific concentration dependence of  $\tau_0$  shown in Figure 3. In fact, the dependence of the delay time of the process on protein concentration has been recently used as a fingerprint for the aggregation mechanism involved. A power law with an exponent significantly higher than  $-0.5$  (in absolute value) has been suggested as a possible indication of the presence of complex secondary nucleation processes including self-catalysis.<sup>28</sup> Specifically, our  $-1.8$  exponent would be close to the one recently found for surface-assisted processes in the A $\beta$ 42 aggregation process.<sup>29</sup> However, we would like to stress that in our model, this effect is detectable only in the proximity of the fibril ends and that a 3D generalization of our framework would be necessary to describe in further detail the occurrence of complex self-catalytic mechanisms also happening in the proximity of the lateral surfaces of the fibrils. Finally, it is worth mentioning that the kinetic cooperativity demonstrated in Figure 4d could be linked to the framework of the dock–lock monomer addition mechanism observed in many instances.<sup>13</sup> This mechanism includes the possibility of monomer addition to a fibril and rearrangement of the monomer in a stable  $\beta$  state within the fibrillar structure.<sup>40</sup>

In summary, we show that our 2D model for amyloid-like fibril formation is able to recover the main features of a fibrillation process. Specifically, we explicitly consider the

change in the geometrical shape of the native monomer undergoing conformational changes (i.e.,  $\Pi$ – $\beta$  transition). Such an early process is linked to the charge state of the side chain of the protein that eventually affects the temporal course of the kinetics. Despite the small number of degrees of freedom, our model allows one to predict the capability of already-formed aggregates to catalyze the conversion of native molecules into aggregation-prone ones, also reproducing scaling laws between meaningful experimental parameters. Although the present model is only valid for fibril formation, a 3D generalization of this framework and the consequential increase of the degrees of freedom would allow one to describe in detail other more complex 3D structures, for example, amyloid particulates and spherulites, often observed during an aggregation process and recently modeled through a coarse-grained hard-sphere approach.<sup>41</sup> This study is currently in progress.

## METHODS

For all of the simulations presented here, we use  $R_h = 4\delta$ ,  $R_{gc} = 3\delta$ ,  $R_{gg} = 2\delta$ ,  $\lambda = 6\delta$ ,  $\epsilon_{gg} = 6k_B T$ ,  $\epsilon_{gc} = 10k_B T$ , and  $\epsilon_d = 10k_B T$ , where  $\delta$  is the reduced unit length, which can be estimated as  $\delta \approx 0.25$  nm,  $k_B$  is the Boltzmann constant, and  $T$  is the temperature. For equilibrium simulations, the parameter  $\epsilon_h$  is kept equal to  $10k_B T$ ; for dynamic simulations, we use  $\epsilon_h = 16k_B T$ . The effect of changing  $\epsilon_h$  in the fibrillation kinetics is shown in Figure S2 (Supporting Information). Whenever not specified, we express lengths and energies in units of  $\delta$  and  $k_B T$ . Charges are expressed in units of  $(k_B T \delta)^{1/2}$ .

Simulations are performed at a constant number of particles  $N$ , temperature, and volume (surface) in a 2D square box of size  $L$  with periodic boundary conditions. The cutoff radius is  $R_C = \min[35\sigma, L/2]$ . Implemented metropolis MC moves include single-protein translations, with a maximum amplitude of  $\Delta r$  in  $x$  and  $y$  directions, rigid rotations of the single proteins with a maximum amplitude of  $\Delta\Phi$ , and rotations of the individual dumbbells with respect to the internal frame of reference of the proteins, with a maximum amplitude of  $\Delta\phi$ . For equilibrium simulations, we chose  $\Delta r = 2\sigma$  and  $\Delta\Phi = \Delta\phi = 2$ .

For the case of dynamic simulations, the step amplitudes are set to small enough values in order to prevent the occurrence of nonphysical moves,  $\Delta r = \sigma$ ,  $\Delta\Phi = 0.125$ , and  $\Delta\phi = 0.25$ . This technique is found to reproduce correctly the dynamics of Brownian objects if hydrodynamic interactions are negligible.<sup>11,42–45</sup> Given the diffusivity of a typical amyloid-forming protein ( $\sim 0.15$  nm<sup>2</sup>/ns),<sup>46</sup> the physical time  $\tau$  corresponding to a MC cycle, in which all of the proteins move (translate) on average once, can be estimated as  $\tau \approx 0.4$  ns. In each MC cycle, all proteins rotate on average once and all dumbbells twice.

The ensembles are initialized on a square lattice with randomly distributed  $\phi_1$  and  $\phi_2$ . The systems are then allowed to equilibrate in a gas phase. During this pre-equilibration stage, fibrillation is hindered by using longer-ranged core–group and group–group steric repulsion, that is, large values of  $R_{gg}$  and  $R_{gc}$ . Because  $V_{gg/gc}$  is only active between different proteins, this choice does not affect the dumbbells' degrees of freedom  $\phi_1$  and  $\phi_2$ , which also reach their equilibrium distribution during the pre-equilibration.

Once the system is equilibrated,  $R_{gg}$  and  $R_{gc}$  are set to the original values of the model, eventually enabling the fibrillation.

## ASSOCIATED CONTENT

### Supporting Information

Normalized mass distribution at equilibrium, aggregation kinetics for large aggregates, and aggregation kinetics with variable  $\epsilon_h$ . This material is available free of charge via the Internet at <http://pubs.acs.org>.

## AUTHOR INFORMATION

### Corresponding Author

\*E-mail: [vito.fodera@sund.ku.dk](mailto:vito.fodera@sund.ku.dk).

### Notes

The authors declare no competing financial interest.

## ACKNOWLEDGMENTS

V.F. acknowledges support from the FP7Marie-Curie Actions Intra European Fellowship (IEF) for Career Development 2012–2014, Project Nr. 299385 “FibCat”, at the University of Copenhagen, Denmark. L.D.M. acknowledges support from the Marie Curie Initial Training Network ITN-COMPLOIDS Grant 234810. The authors thank Valeria Vetri (University of Palermo) for critical reading. This work was performed using the Darwin Supercomputer of the University of Cambridge High Performance Computing Service.

## REFERENCES

- (1) Chiti, F.; Webster, P.; Taddei, N.; Clark, A.; Stefani, M.; Ramponi, G.; Dobson, C. M. Designing Conditions for In Vitro Formation of Amyloid Protofilaments and Fibrils. *Proc. Natl. Acad. Sci. U.S.A.* **1999**, *96*, 3590–3594.
- (2) Vendruscolo, M.; Zurdo, J.; MacPhee, C. E.; Dobson, C. M. Protein Folding and Misfolding: a Paradigm of Self-Assembly and Regulation in Complex Biological System. *Phil. Trans. R. Soc. London, Ser. A* **2003**, *361*, 1205–1222.
- (3) Griffin, M. D. W.; Mok, M. L. Y.; Wilson, L. M.; Pham, C. L. L.; Waddington, L. J.; Perugini, M. A.; Howlett, G. J. Phospholipid Interaction Induces Molecular-Level Polymorphism in Apolipoprotein C-II Amyloid Fibrils via Alternative Assembly Pathways. *J. Mol. Biol.* **2008**, *375*, 240–256.
- (4) Pellarin, R.; Cafilisch, A. Interpreting the Aggregation Kinetics of Amyloid Peptides. *J. Mol. Biol.* **2006**, *360*, 882–892.
- (5) Friedman, R.; Pellarin, R.; Cafilisch, A. Amyloid Aggregation on Lipid Bilayers and Its Impact on Membrane Permeability. *J. Mol. Biol.* **2009**, *387*, 407–415.
- (6) Friedman, R.; Pellarin, R.; Cafilisch, A. Soluble Protofibrils as Metastable Intermediates in Simulations of Amyloid Fibril Degradation Induced by Lipid Vesicles. *J. Phys. Chem. Lett.* **2009**, *1*, 471–474.
- (7) Gaspari, R.; Gliozzi, A.; Ferrando, R. Aggregation Phenomena in a System of Molecules with Two Internal States. *Phys. Rev. E* **2007**, *76*, 041604.
- (8) Strodel, B.; Wales, D. J. Implicit Solvent Models and the Energy Landscape for Aggregation of the Amyloidogenic KFFE Peptide. *J. Chem. Theory Comput.* **2008**, *4*, 657–672.
- (9) Vacha, R.; Frenkel, D. Relation between Molecular Shape and the Morphology of Self-Assembling Aggregates: A Simulation Study. *Biophys. J.* **2011**, *101*, 1432–1439.
- (10) Irbäck, A.; Jónsson, S. Æ.; Linnemann, N.; Linse, B.; Wallin, S. Aggregate Geometry in Amyloid Fibril Nucleation. *Phys. Rev. Lett.* **2013**, *110*, 058101.
- (11) Bieler, N. S.; Knowles, T. P. J.; Frenkel, D.; Vacha, R. Connecting Macroscopic Observables and Microscopic Assembly Events in Amyloid Formation Using Coarse Grained Simulations. *PLoS Comput. Biol.* **2012**, *8*, e1002692.
- (12) Whitelam, S.; Rogers, C.; Pasqua, A.; Paavola, C.; Trent, J.; Geissler, P. L. The Impact of Conformational Fluctuations on Self-Assembly: Cooperative Aggregation of Archaeal Chaperonin Proteins. *Nano Lett.* **2009**, *9*, 292–297.



- (13) Nguyen, P. H.; Li, M. S.; Stock, G.; Straub, J. E.; Thirumalai, D. Monomer Adds to Preformed Structured Oligomers of  $\alpha\beta$ -Peptides by a Two-Stage Dock-Lock Mechanism. *Proc. Natl. Acad. Sci. U.S.A.* **2007**, *104*, 111–116.
- (14) Baiesi, M.; Seno, F.; Trovato, A. Fibril Elongation Mechanisms of HET-s Prion-Forming Domain: Topological Evidence for Growth Polarity. *Proteins: Struct., Funct., Bioinf.* **2011**, *79*, 3067–3081.
- (15) Buell, A. K.; Blundell, J. R.; Dobson, C. M.; Welland, M. E.; Terentjev, E. M.; Knowles, T. P. J. Frequency Factors in a Landscape Model of Filamentous Protein Aggregation. *Phys. Rev. Lett.* **2010**, *104*, 228101.
- (16) Wu, C.; Shea, J.-E. Coarse-Grained Models for Protein Aggregation. *Curr. Opin. Struct. Biol.* **2011**, *21*, 209–220.
- (17) Yong, W.; Lomakin, A.; Kirkitadze, M. D.; Teplow, D. B.; Chen, S.-H.; Benedek, G. B. Structure Determination of Micelle-Like Intermediates in Amyloid  $\beta$ -Protein Fibril Assembly by Using Small Angle Neutron Scattering. *Proc. Natl. Acad. Sci. U.S.A.* **2002**, *99*, 150–154.
- (18) Lomakin, A.; Chung, D. S.; Benedek, G. B.; Kirschner, D. A.; Teplow, D. B. On the Nucleation and Growth of Amyloid  $\beta$ -Protein Fibrils: Detection of Nuclei and Quantitation of Rate Constants. *Proc. Natl. Acad. Sci. U.S.A.* **1996**, *93*, 1125–1129.
- (19) Li, M. S.; Klimov, D. K.; Straub, J. E.; Thirumalai, D. Probing the Mechanisms of Fibril Formation Using Lattice Models. *J. Chem. Phys.* **2008**, *129*, 175101/1–175101/10.
- (20) Li, M. S.; Co, N. T.; Reddy, G.; Hu, C.-K.; Straub, J. E.; Thirumalai, D. Factors Governing Fibrillogenesis of Polypeptide Chains Revealed by Lattice Models. *Phys. Rev. Lett.* **2010**, *105*, 218101.
- (21) Massi, F.; Klimov, D.; Thirumalai, D.; Straub, J. E. Charge States Rather than Propensity for  $\beta$ -Structure Determine Enhanced Fibrillogenesis in Wild-Type Alzheimer's-Amyloid Peptide Compared to E22Q Dutch Mutant. *Protein Sci.* **2002**, *11*, 1639–1647.
- (22) Vetri, V.; Militello, V. Thermal Induced Conformational Changes Involved in the Aggregation Pathways of  $\beta$ -Lactoglobulin. *Biophys. Chem.* **2005**, *113*, 83–91.
- (23) Vetri, V.; Canale, C.; Relini, A.; Librizzi, F.; Militello, V.; Gliozi, A.; Leone, M. Amyloid Fibrils Formation and Amorphous Aggregation in Concanavalin A. *Biophys. Chem.* **2007**, *125*, 184–190.
- (24) Vetri, V.; D'Amico, M.; Foderà, V.; Leone, M.; Ponzoni, A.; Sberveglieri, G.; Militello, V. Bovine Serum Albumin Protofibril-Like Aggregates Formation: Solo but Not Simple Mechanism. *Arch. Biochem. Biophys.* **2011**, *508*, 13–24.
- (25) Librizzi, F.; Foderà, V.; Vetri, V.; Lo Presti, C.; Leone, M. Effects of Confinement on Insulin Amyloid Fibrils Formation. *Eur. Biophys. J.* **2007**, *36*, 711–715.
- (26) Foderà, V.; Librizzi, F.; Groenning, M.; van de Weert, M.; Leone, M. Secondary Nucleation and Accessible Surface in Insulin Amyloid Fibril Formation. *J. Phys. Chem. B* **2008**, *112*, 3853–3858.
- (27) Foderà, V.; van de Weert, M.; Vestergaard, B. Large-Scale Polymorphism and Auto-Catalytic Effect in Insulin Fibrillogenesis. *Soft Matter* **2010**, *6*, 4413–4419.
- (28) Knowles, T. P. J.; Waudby, C. A.; Devlin, G. L.; Cohen, S. I. A.; Aguzzi, A.; Vendruscolo, M.; Terentjev, E. M.; Welland, M. E.; Dobson, C. M. An Analytical Solution to the Kinetics of Breakable Filament Assembly. *Science* **2009**, *326*, 1533–1537.
- (29) Cohen, S. I. A.; Linse, S.; Luheshi, L. M.; Hellstrand, E.; White, D. A.; Rajah, L.; Otzen, D. E.; Vendruscolo, M.; Dobson, C. M.; Knowles, T. P. J. Proliferation of Amyloid- $\beta$ 42 Aggregates Occurs through a Secondary Nucleation Mechanism. *Proc. Natl. Acad. Sci. U.S.A.* **2013**, DOI: 10.1073/pnas.1218402110.
- (30) Wood, S. J.; Maleeff, B.; Hart, T.; Wetzel, R. Physical, Morphological and Functional Differences between pH 5.8 and 7.4 Aggregates of the Alzheimer's Amyloid Peptide  $A\beta$ . *J. Mol. Biol.* **1996**, *256*, 870–877.
- (31) Schmittschmitt, J. P.; Scholtz, J. M. The Role of Protein Stability, Solubility, and Net Charge in Amyloid Fibril Formation. *Protein Sci.* **2003**, *12*, 2374–2378.
- (32) Hoyer, W.; Antony, T.; Cherny, D.; Heim, G.; Jovin, T. M.; Subramaniam, V. Dependence of  $\alpha$ -Synuclein Aggregate Morphology on Solution Conditions. *J. Mol. Biol.* **2002**, *322*, 383–393.
- (33) Haas, J.; Vöhringer-Martinez, E.; Bögehold, A.; Matthes, D.; Hensen, U.; Pelah, A.; Abel, B.; Grubmüller, H. Primary Steps of pH-Dependent Insulin Aggregation Kinetics Are Governed by Conformational Flexibility. *ChemBioChem* **2009**, *10*, 1742–1742.
- (34) Smith, M. I.; Foderà, V.; Sharp, J. S.; Roberts, C. J.; Donald, A. M. Factors Affecting the Formation of Insulin Amyloid Spherulites. *Colloids Surf., B* **2012**, *89*, 216–222.
- (35) Fändrich, M. Absolute Correlation between Lag Time and Growth Rate in the Spontaneous Formation of Several Amyloid-Like Aggregates and Fibrils. *J. Mol. Biol.* **2007**, *365*, 1266–1270.
- (36) Jansen, R.; Dzwolak, W.; Winter, R. Amyloidogenic Self-Assembly of Insulin Aggregates Probed by High Resolution Atomic Force Microscopy. *Biophys. J.* **2005**, *88*, 1344–1353.
- (37) Ferrone, F. A.; Hofrichter, J.; Eaton, W. A. Kinetics of Sick Hemoglobin Polymerization: I. Studies Using Temperature-Jump and Laser Photolysis Techniques. *J. Mol. Biol.* **1985**, *183*, 591–610.
- (38) Ferrone, F. A.; Hofrichter, J.; Eaton, W. A. Kinetics of Sick Hemoglobin Polymerization: II. A Double Nucleation Mechanism. *J. Mol. Biol.* **1985**, *183*, 611–631.
- (39) Foderà, V.; Cataldo, S.; Librizzi, F.; Pignataro, B.; Spiccia, P.; Leone, M. Self-Organization Pathways and Spatial Heterogeneity in Insulin Amyloid Fibril Formation. *J. Phys. Chem. B* **2009**, *113*, 10830–10837.
- (40) O'Brien, E. P.; Okamoto, Y.; Straub, J. E.; Brooks, B. R.; Thirumalai, D. Thermodynamic Perspective on the Dock-Lock Growth Mechanism of Amyloid Fibrils. *J. Phys. Chem. B* **2009**, *113*, 14421–14430.
- (41) Foderà, V.; Zacccone, A.; Lattuada, M.; Donald, A. M. Electrostatics Controls the Formation of Amyloid Superstructures in Protein Aggregation. *Phys. Rev. Lett.* **2013**, *111*, 108105.
- (42) Kikuchi, K.; Yoshida, M.; Maekawa, T.; Watanabe, H. Metropolis Monte Carlo Method as a Numerical Technique to Solve the Fokker–Planck Equation. *Chem. Phys. Lett.* **1991**, *185*, 335–338.
- (43) Fichtthorn, K. A.; Weinberg, W. H. Theoretical Foundations of Dynamical Monte Carlo Simulations. *J. Chem. Phys.* **1991**, *95*, 1090–1096.
- (44) Whitelam, S.; Geissler, P. L. Avoiding Unphysical Kinetic Traps in Monte Carlo Simulations of Strongly Attractive Particles. *J. Chem. Phys.* **2007**, *127*, 154101.
- (45) Sanz, E.; Marenduzzo, D. Dynamic Monte Carlo versus Brownian Dynamics: A Comparison for Self-Diffusion and Crystallization in Colloidal Fluids. *J. Chem. Phys.* **2010**, *132*, 194102–7.
- (46) Bora, R. P.; Prabhakar, R. Translational, Rotational and Internal Dynamics of Amyloid  $\beta$ -Peptides ( $A\beta$ 40 and  $A\beta$ 42) from Molecular Dynamics Simulations. *J. Chem. Phys.* **2009**, *131*, 155103/1–133103/11.